Stapler Design with Stacked Tensegrity Mechanisms for Surgical Procedures

Dhruva Khanzode, Ranjan Jha, Damien Chablat, Emilie Duchalais

**The ASME 2022 International Design Engineering Technical Conferences &
Computers and Information in Engineering Conference
IDETC/CIE 2022
August 14–172022Saint LouisUSA**

DETC2022/MR-89714

STAPLER DESIGN WITH STACKED TENSEGRITY MECHANISMS FOR SURGICAL PROCEDURES

Dhruva Khanzode, Ranjan Jha
BioMedical Application Division, CSIR
Central Scientific Instruments Organisation
Academy of Scientific and Innovative Research
(AcSIR),Chandigarh, India
Emails: khanzode.dhruva@csio.res.in,
ranjan.jha@csio.res.in

Damien Chablat
Laboratoire des Sciences
du Numérique de Nantes,
UMR CNRS 6004, Nantes, France
Email: damien.chablat@cnrs.fr

Emilie Duchalais
CHU Nantes
Centre hospitalier universitaire de Nantes
France
Email: emilie.dassonneville@chu-nantes.fr

ABSTRACT

In this paper, a planar mechanism formed by stacking tensegrity mechanisms has been designed. This mechanism is formed by three segments but the approach can be applied to a larger number of segments. This mechanism is studied to serve as a stapler for laparoscopic rectal cancer surgery where conventional tools cannot be easily accessed. To do this, two identical mechanisms will be used and operated similarly: one to carry the clips and the cutting knife and the second in parallel to allow the closing of the clips by bringing the two mechanisms together. The parameterization of the segments allows a variation of all lengths. Thus, the size of the segments can decrease proportionally from the base to the top, resulting in a tapered shape from the base to the tip like an elephant trunk. The mechanism has linear springs and cables for its actuation. The singularities, as well as the stability of the parallel mechanism, were analyzed using the minimum energy principle. Optimization was also performed to obtain the largest angular deflection for a segment based on a ratio between the size of the base and the moving platform of the robotic system. The result of this work is a family of mechanisms that can generate the same workspace for different stability properties. After optimization, the radius of curvature of the mechanism will be studied to allow insertion into the patient's belly.

INTRODUCTION

The field of medical science has grown leaps and bounds in the last century. The advancement in technology and the introduction of newer devices and machines have made the life of a doctor easier from time to time. Currently, this facility is provided by robotic systems. Nowadays, robotic systems are being used in various fields of medical science, may it be diagnosis, drug delivery, or surgery. One such device introduced approximately a century ago is a surgical stapler [1]. The first surgical stapler was invented in 1908 by Victor Fischer and Hümér Hültl. This device was initially developed to prevent the risk of infection due to spillage of Gastro-Intestinal contents on the wounds of the patients undergoing abdominal surgeries. The idea was to seal and shut the hollow organs before their division, hence preventing the spillage. The surgical stapler was then called a “mechanical stitching device" [2]. The device used 4 rows of U-shaped staples of steel wires for a length of 17cm and 11 cm. The two design parameters that are still used in modern surgical staplers was the final B shape of the staple [3] which allowed blood flow through the tissue and the staggered arrangement of the staple pins [4]. This design was known as “Fischer- Hültl stapler”. Since its invention in 1908, various modifications were made to the design through the 1960s and several researchers such as Aladár Petz and H. Friedrich contributed a lot to the research, such as developing an “L” shape stapler as a successor to linear staplers. The first modern stapler was invented in 1964 by Mark Ravitch, Leon

Hirsch, and Felicien Steichen under the banner of United States Surgical Corporation (USSC). This device first introduced the use of disposable staple cartridges. Along with this, they also developed surgical staplers with a circular stapling area. The USSC products became so popular that their acronyms are still used as a part of surgical vocabulary such as TA, thoracoabdominal; GIA, GI anastomosis. With such success, a competitor named Ethicon appeared in 1997, which was then and still is a subsidiary of Johnson & Johnson brand and USSC itself successively became Covidien, which is now a part of medical & healthcare giant Medtronics.

In today's surgeries, generally, five kinds of staplers are used, namely TA, Thorasic-Abdominal; GIA, Gastro-Intestinal Anastomosis; Endo GIA, Endoscopic Gastro-Intestinal Anastomosis; EEA, End-End Anastomosis and Skin Stapler. The TA stapler is not equipped with a knife to cut the tissue after the firing of stapler pins and hence the tissue needs to be separated manually. The EEA stapler provides circular staples [5] and the skin stapler is used to close superficial wounds. The TA stapler is most prominently used in veterinary surgical procedures [6]. GIA and Endo GIA are the most used staplers for abdominal surgeries and the Endo GIA staplers are specifically used for minimally invasive surgical procedures [7]. Presently, the Endo GIA staplers are available in 3 forms: passive articulated wrist type (PAW) [8], active articulated wrist type (AAW) [9], and radial reload type staplers (RR). In PAW, the desired bending of the wrist is achieved by pressing the jaw upon the abdominal wall, whereas in AAW, a lever is provided to articulate the wrist into pre-determined bending angles. RR comes with a fixed "U" shape jaw and has been proven to be very useful for pulmonary surgeries [10]. The RR type stapler is only commercialized by Covidien Inc. The main drawback of the RR type stapler is that it requires a very large incision to enter the body and hence defeats the purpose of "minimally invasive surgery" [11]. Hence there is a dire need for a surgical stapler that can enter through the laparoscopic openings, but can work as a RR type stapler inside the body.

The article is organized as follows. In section 2, the problem of surgical staplers for coloanal anastomosis is introduced to present the need for surgeons. In section 3, the kinematics of the studied mechanism is presented. Section 4 reports the different computational results to study the singularities associated with the mechanism, then in section 5, the study of stability based on the principle of minimum energy, and finally, in section 6, an optimization of the dimensions of the mechanism is presented. Section 7 presents simulations for three mechanism designs to achieve bending by cable contraction taking into account the no-load length of the springs.

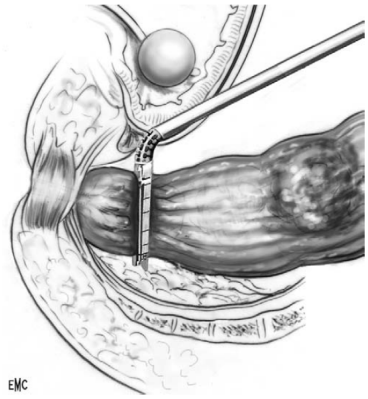

FIGURE 1. Placement of a clamp on the rectum under the tumour [12].

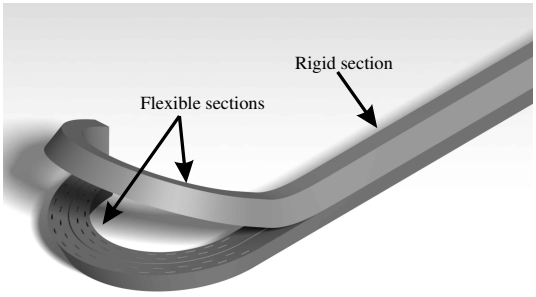

FIGURE 2. New stapler design with flexible sections

SURGICAL STAPLERS FOR COLOANAL ANASTOMOSIS

The surgery uses many tools during coloanal anastomosis. Classically, a rectal clamp is placed under the tumour and the rectum is closed transversely below the clamp using a linear clamp or an articulated clamp and then cut flush with the mechanical clamp with a scalpel. In this constrained environment, located between the spine and the bladder, the prostate for men, or the uterus for women, the accessibility of tools is difficult. In addition, depending on the gender and weight of the patient, the workspace changes and the tools have to adapt to a more or less rigid environment [12]. It should also be noted that the stapler is introduced into the peritoneal cavity through the right lower trocar. This limits the volume of the tools but also requires a slender shape to pass through the trocar [13]. The objective of our study is to design a stenting tool that can be inserted through the trocar in a straight line and then bent to fit the colon over a variable width depending on the patient's anatomy. The actuation will be done by two cables which will ensure the obtaining of the good curvature and the stability during the stapling then the cutting of the colon. Two flexible sections will be designed using staked tensegrity structures as shown in Fig. 2

MECHANISM DESIGN OF THE TENSEGRITY STRUCTURE

In this article, the robotic system designed is a 2 DOF multi-segment planar robotic system. As depicted in Fig. 3, the robotic system comprises of three trapezoidal segments Ⓐ, Ⓑ and Ⓒ, stacked one above the other. Each segment may have a larger base plate and a smaller moving plate. Both the plates are connected by a central serial spine linkage, comprising of three links.

For example, in segment Ⓐ, the central spinal linkages are (A_0B_0), (B_0C_0) and (C_0D_0). The link A_0B_0 and C_0D_0 are rigidly fixed and are perpendicular to their respective plate (A_1A_2) and (D_1D_2). These central spinal links are connected by two revolute joints with identical rotation angles. To achieve this coupling, the joints can have a sliding surface, similar to a knee joint in humans, or can also have an X-shape tensegrity module [14, 15], or a gear train to couple the movement of the two revolute joints.

The base plate and the moving plates are also attached with the help of two cables ρ_1 and ρ_2, present on either side of the central spine and two springs of stiffness k_1 and k_2 between $(A_1\ D_1)$ and $(A_2\ D_2)$, respectively.

The contraction of the cables will stimulate angular displacement in the revolute joints of the central spine and replication of this phenomenon in each of the three segments will eventually facilitate the bending of the robotic structure. The length of the cable is measured as ρ_i and the angular deviation of the revolute joints is measured as α_i where

$$\alpha_1 = \alpha_2, \quad \alpha_3 = \alpha_4, \quad \alpha_5 = \alpha_6, \tag{1}$$

because of the coupling inside each segment.

The fixed coordinate frame of the base is represented by Σ_0 with the origin at A_0. The distances between the coordinates of each points are $||\mathbf{a}_1 - \mathbf{a_0}|| = \mathbf{l_1}$, $||\mathbf{a}_2 - \mathbf{a_0}|| = \mathbf{l_1}$, $||\mathbf{b}_0 - \mathbf{a_0}|| = \mathbf{h_1}$, $||\mathbf{c}_0 - \mathbf{b_0}|| = \mathbf{h_2}$, $||\mathbf{d}_0 - \mathbf{c_0}|| = \mathbf{h_3}$, $||\mathbf{d}_1 - \mathbf{d_0}|| = \mathbf{l_2}$ and $||\mathbf{d}_2 - \mathbf{d_0}|| = \mathbf{l_2}$ for Ⓐ. For Ⓑ, we have $||\mathbf{e}_0 - \mathbf{d_0}|| = \mathbf{h_4}$, $||\mathbf{f}_0 - \mathbf{e_0}|| = \mathbf{h_5}$, $||\mathbf{g}_0 - \mathbf{f_0}|| = \mathbf{h_6}$, $||\mathbf{g}_1 - \mathbf{g_0}|| = \mathbf{l_3}$ and $||\mathbf{g}_2 - \mathbf{g_0}|| = \mathbf{l_3}$. Finally, For Ⓒ, we have $||\mathbf{h}_0 - \mathbf{g_0}|| = \mathbf{h_7}$, $||\mathbf{i}_0 - \mathbf{h_0}|| = \mathbf{h_8}$, $||\mathbf{j}_0 - \mathbf{h_0}|| = \mathbf{h_9}$, $||\mathbf{j}_1 - \mathbf{j_0}|| = \mathbf{l_4}$ and $||\mathbf{g}_2 - \mathbf{g_0}|| = \mathbf{l_4}$.

The vector co-ordinates for the base mounting points are given by

$$\mathbf{a}_1 = [-l_1, 0] \quad \mathbf{a}_2 = [l_1, 0] \tag{2}$$

The kinematic chain between the base and the platform of the

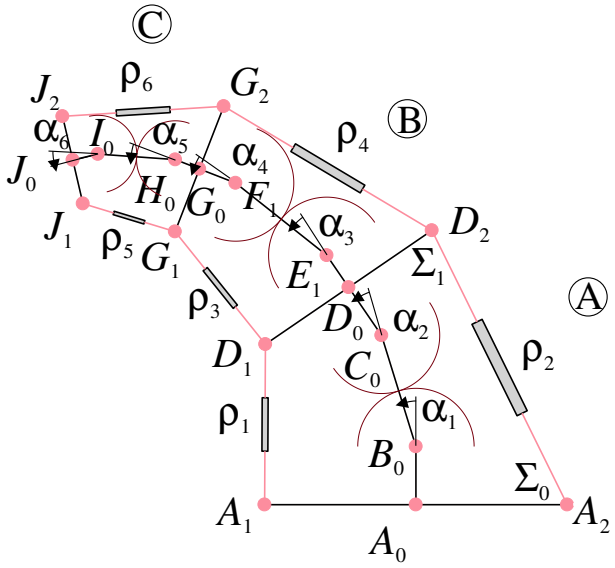

FIGURE 3. The tensegrity mechanism understudy with three segments stacked, named Ⓐ, Ⓑ, Ⓒ for $\alpha_i = 0.3$ in the right

first segment is defined by the following points

$$\mathbf{b}_0 = \begin{bmatrix} 0 \\ h_1 \end{bmatrix},$$
$$\mathbf{c}_0 = \begin{bmatrix} -h_2 \sin(\alpha_1) \\ h_1 + h_2 \cos(\alpha_1) \end{bmatrix},$$
$$\mathbf{d}_0 = \begin{bmatrix} -h_2 \sin(\alpha_1) - h_3 \sin(2\alpha_1) \\ h_1 + h_2 \cos(\alpha_1) + h_3 \cos(2\alpha_1) \end{bmatrix} \tag{3}$$

The moving co-ordinate frame of the first segment is represented by Σ_1 with its origin at D_0. The spring mounting points are represented by D_1 and D_2.

$$\mathbf{d}_1 = \begin{bmatrix} (-2h_3 \cos(\alpha_1) - h_2) \sin(\alpha_1) - 2l_2 \cos^2(\alpha_1) + l_2 \\ 2h_3 \cos^2(\alpha_1) + (h_2 - 2l_2 \sin(\alpha_1)) \cos(\alpha_1) + h_1 - h_3 \end{bmatrix} \tag{4}$$
$$\mathbf{d}_2 = \begin{bmatrix} (-2h_3 \cos(\alpha_1) - h_2) \sin(\alpha_1) + 2l_2 \cos^2(\alpha_1) - l_2 \\ 2h_3 \cos^2(\alpha_1) + (h_2 + 2l_2 \sin(\alpha_1)) \cos(\alpha_1) + h_1 - h_3 \end{bmatrix} \tag{5}$$

The inverse kinematic model for a segment is used to determine the length of the springs and the cables between the base and the moving platform and the moving platform. The equations are given by

$$||\mathbf{a}_1 - \mathbf{d}_1|| = \rho_1, \quad ||\mathbf{a}_2 - \mathbf{d}_2|| = \rho_2 \tag{6}$$

These two equations can also be written as

$$\left((-2h_3\cos(\alpha_1)-h_2)\sin(\alpha_1)-2l_2\left(\cos^2(\alpha_1)\right)+l_2+l_1\right)^2 \quad (7)$$
$$+\left(2h_3\left(\cos^2(\alpha_1)\right)+(-2l_2\sin(\alpha_1)+h_2)\cos(\alpha_1)+h_1-h_3\right)^2=\rho_1^2$$
$$\left((-2h_3\cos(\alpha_1)-h_2)\sin(\alpha_1)+2l_2\left(\cos^2(\alpha_1)\right)-l_2-l_1\right)^2 \quad (8)$$
$$+\left(2h_3\left(\cos^2(\alpha_1)\right)+(2l_2\sin(\alpha_1)+h_2)\cos(\alpha_1)+h_1-h_3\right)^2=\rho_2^2$$

For Ⓑ and Ⓒ, we can write in the same way the positions of the joints. The inverse kinematic model is given by

$$||\mathbf{d}_1-\mathbf{g}_1||=\rho_3,\quad ||\mathbf{d}_2-\mathbf{g}_2||=\rho_4 \quad (9)$$
$$||\mathbf{g}_1-\mathbf{j}_1||=\rho_5,\quad ||\mathbf{g}_2-\mathbf{j}_2||=\rho_6 \quad (10)$$

where ρ_3, ρ_4, k_3 and k_4 define the length of the cable and the stiffness of the springs between (G_1 D_1) and (G_2 D_2), respectively, and ρ_5, ρ_6, k_5 and k_6 define the length of the cable and the stiffness of the springs between (J_1 G_1) and (J_2 G_2), respectively.

SINGULARITY ANALYSIS

For determining the singularities of the multi-segment planar mechanism, only the segment Ⓐ was taken into consideration. As all other sections are similarly constructed, analysis of singularities in one section will lead to similar results in all other sections.

Two closed-loop mechanisms can be described by (A_1, A_0, B_0, C_0, D_0, D_1) and (A_2, A_0, B_0, C_0, D_0, D_2). For the first closed-loop mechanism, the singular configurations with α_1 as Cartesian values and ρ_1 as the input values are computed by differentiating with respect to time the Eq. 8, as follow,

$$\begin{aligned}&-8h_3^2C_{\alpha_1}^3S_{\alpha_1}+8h_3^2C_{\alpha_1}S_{\alpha_1}-8l_2^2C_{\alpha_1}^3S_{\alpha_1}+8l_2^2C_{\alpha_1}S_{\alpha_1}\\&-4h_3S_{\alpha_1}C_{\alpha_1}^2h_2-4h_3S_{\alpha_1}^3h_2-4h_3C_{\alpha_1}^2l_1+4h_3S_{\alpha_1}^2l_1\\&-4l_2C_{\alpha_1}^2h_1+4l_2S_{\alpha_1}^2h_1-8h_3^2S_{\alpha_1}^3C_{\alpha_1}-2h_2C_{\alpha_1}l_2\\&-2h_2C_{\alpha_1}l_1+8l_2C_{\alpha_1}l_1S_{\alpha_1}-8l_2^2S_{\alpha_1}^3C_{\alpha_1}-8h_3C_{\alpha_1}h_1S_{\alpha_1}\\&-2h_2S_{\alpha_1}h_1+2h_2S_{\alpha_1}h_3=0\end{aligned} \quad (11)$$

where, $C_{\alpha_1}=\cos(\alpha_1)$ and $S_{\alpha_1}=\sin(\alpha_1)$ respectively. The singularities are the roots of a 4th-degree equation. When $l_1\neq l_2$, only a numerical method allows us to calculate them. In our case, we use the "RootFinding:-Isolate" function of Maple which computes all the roots after a substitution by the half-angle of α_1 to obtain an algebraic equation [16].

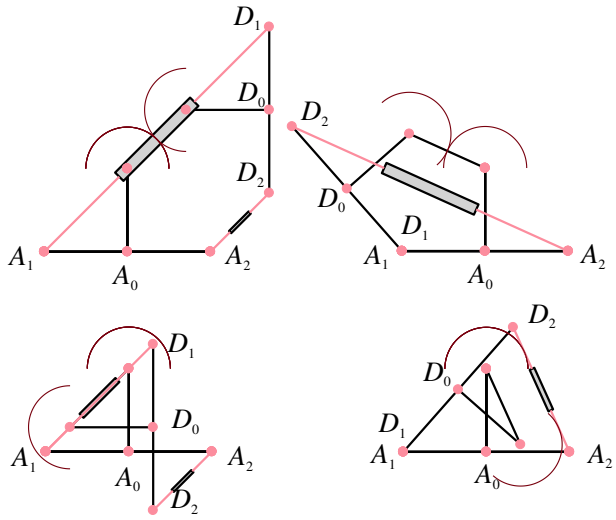

FIGURE 4. Four singular configurations for $h_1=1, h_2=1, h_3=1, l_1=1$ and $l_2=1$

For the second closed-loop, the singularity locus is for opposite values of α_1. For each closed loop, there can be up to four singular positions. The absolute value of the smallest angle α_i is called α_{sing} and it represents the largest travel that the mechanism can achieve. This value must be maximized.

As an example, for $h_1=1$, $h_2=1$, $h_3=1$, $l_1=1$, $l_2=1$, the singularity locus are

$$\begin{aligned}\alpha_1&=-\frac{\pi}{4},\alpha_1=\frac{3\pi}{4}\\ \alpha_1&=\arctan\left(\frac{\frac{1}{4}+\frac{\sqrt{7}}{4}}{-\frac{1}{4}+\frac{\sqrt{7}}{4}}\right),\alpha_1=\arctan\left(\frac{\frac{1}{4}-\frac{\sqrt{7}}{4}}{-\frac{1}{4}-\frac{\sqrt{7}}{4}}\right)-\pi\end{aligned} \quad (12)$$

Only two singular configurations are close to the home pose as shown in Fig. 4. The smallest absolute value of α_1 defines the range of motion of the segment in both directions.

STABILITY ANALYSIS

The stability of the robotic system is one of the major elements in the evaluation of its performance [17]. In general, when a system is in equilibrium and is moved by an external force if the system returns to its equilibrium state, it is called a stable equilibrium. If the system does not return to equilibrium, it is considered an unstable system [18]. A robotic system is always desired to be naturally stable without control. If a robotic system becomes unstable at any point in its trajectory, then it may cause substantial errors during its control [19]. For this 2 DOF multi-segment planar robotic system, the stability is evaluated by using the principle of minimum internal energy.

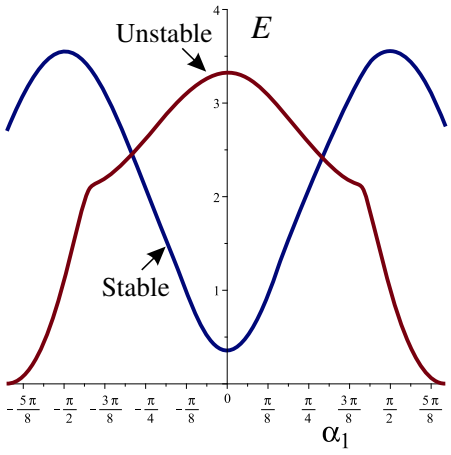

FIGURE 5. Variation of the energy as a function of α_1 for a stable home pose for $h_1 = 0$, $h_2 = 1$, $h_3 = 0$, $l_1 = 1$, $l_2 = 1$, $k = 1$ and unstable home pose for $h_1 = 1$, $h_2 = 1$, $h_3 = 1$, $l_1 = 1$, $l_2 = \frac{1}{2}$, $k = 1$

For the segment Ⓐ, two springs are connected between (A_1D_1) and (A_2D_2) with a no-load length equal to l_{01} and l_{01}, respectively. This length is chosen as 40% of the length in the home pose. This value will be proportional to the size of the second and third segments if we want to characterize the stability of the complete mechanism.

For the segment Ⓐ, the energy E for a given α inside the mechanism is

$$E = \frac{1}{2}\left(k_1(\rho_1 - l_{01})^2 + k_2(\rho_2 - l_{02})^2\right) \tag{13}$$

To compare two mechanisms, we introduce the total energy as $E_t = \int_{-\alpha_{sing}}^{\alpha_{sing}} E$.

Depending on the sizes of the robot, several stability schemes can appear either stable around $\alpha = 0$ up to the singularities or unstable in the position for $\alpha = 0$ (Fig. 5.

OPTIMIZATION OF ONE SEGMENT

The objective of our optimization is to find the design parameters that allow the greatest angular deflection and then to study the stability of the solutions found. A ratio λ between the base and the platform is also studied to see if elephant trunk structures, with sections of decreasing sizes, are relevant [20].

So, the objective function is defined as

$$f(\mathbf{x}) = \alpha_{sing} \rightarrow \max \tag{14}$$

where $\mathbf{x}$ is the set of the design parameters $[h_1, h_2, h_3, l_1, \lambda]$. To simplify the optimization, we set $h_3 = h_1$, $l_2 = \lambda l_1$ and we defined

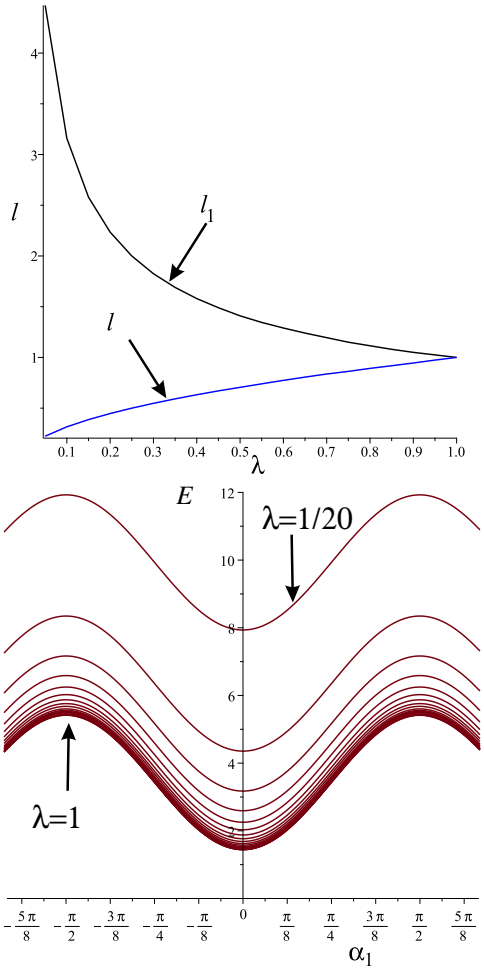

FIGURE 6. Variation of l_1 in black and l_2 in blue as a function of λ (left) and the stability analysis of the optimal solutions as a function of λ

the following constraints:

$$0 < l_1 < 4.5 \quad 0 \le h_1 \le 1 \quad 0 \le h_2 \le 2 \quad 1/20 \le \lambda \le 1 \tag{15}$$

The solution to this optimization problem can be achieved by several methods. As the dimension of the problem is small, a discretization of the parameter space has been performed to find the optimal solutions.

The results of the optimization show that the maximum value of α is $\pi/2$ and this for any value of λ and for $l_2 = 2$, i.e. the maximum bound, and for $h_1 = 0$ for the minimum bound. Figure 6 shows the evolution of l_1 and l_2 as a function of λ.

For all solutions, the energy has its maximum value for α_{sing} and has a local minimum for $\alpha = 0$. If we observe the value of $E(\alpha = 0)$ and $E(\alpha = \pi/2)$, the difference is always the same. The total energy decreases when λ tends to 1. This means that the actuation forces will be smaller when $\lambda = 1$. Conversely, the

smaller λ is, the greater the external forces must be to move the mechanism from its home position. Moreover, to have a regular stack of segments, © is smaller than ® which is smaller than Ⓐ if λ is different from 1.

BENDING SIMULATION

Unlike robots that have an end effector, the purpose of our work is to design a mechanism that will carry staples along its entire length. It is the curvature of the mechanism that will be studied and not the position of its effector.

We will study two mechanisms from the previous optimization with two values of λ and for a mechanism unstable at the home pose.

By using only two cables with one end on the end of the mechanism and the reel on the base, the stable position of the mechanism is achieved by minimizing the energy E_s of the springs of the stacked mechanism.

$$\begin{aligned} E_s = & \frac{1}{2}\left(k_1(\rho_1 - l_{01})^2 + k_2(\rho_2 - l_{02})^2\right) \\ & + \frac{1}{2}\left(k_3(\rho_3 - l_{03})^2 + k_4(\rho_4 - l_{04})^2\right) \\ & + \frac{1}{2}\left(k_5(\rho_5 - l_{05})^2 + k_2(\rho_6 - l_{06})^2\right) \end{aligned} \tag{16}$$

where the no-load lengths of the springs ρ_i are l_{0i}.

The movements are obtained by assigning the length of a single cable and looking for the stable position of the mechanism. We define $\rho_{135} = \rho_1 + \rho_3 + \rho_5$ as the length of the actuated cable and $\rho_{246} = \rho_2 + \rho_4 + \rho_6$ as the passive one. It is not a force control. The inverse kinematic model is used to evaluate ρ_{246}. In this case, only the cable driving the structure is naturally under tension. It is the springs that tend to make the structure return to its home position. The other one is not used to ensure stability.

The problem to be solved is to minimize E_t as a function of ρ_{135} under the constraint of $\rho_i > l_{0i}$. The "LPSolve" command from Maple Software solves a linear program (LP), which involves computing the minimum of a linear objective function subject to linear constraints. The no-load length of each spring ρ_{0i} is determined for $\alpha_i = 0$, for $i = 1, \ldots, 6$.

When $\lambda = 1$, all springs are identical. When a cable is pulled, the energy is equally distributed among the six springs, which causes the mechanism to bend regularly, as shown in Fig. 7.

In the other cases, while the stiffness and percentage of the non-load length of each spring remain the same, the energy in the six springs varies. The smaller springs have less elastic energy than the larger ones.

Figure 7 shows two examples of mechanisms with $\lambda = 1$ for case ① and $\lambda = 0.7$ for case ②.

Figure 8 presents the variation of E_s as a function of ρ_{135}. For ①, the values of E_s are higher and the three angles α_i are

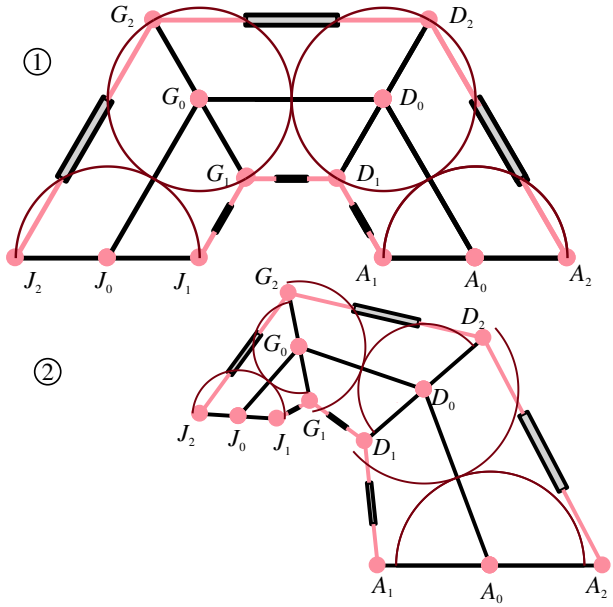

FIGURE 7. Example of bending for two mechanisms with ① $h_1 = 0$, $h_2 = 2$, $h_3 = 0$, $h_4 = 0$, $h_5 = 2$, $h_6 = 0$, $h_7 = 0$, $h_8 = 2$, $h_9 = 0$, $l_1 = 1$, $l_2 = 1$, $l_3 = 1$, $l_4 = 1$ and ② $h_1 = 0$, $h_2 = 2$, $h_3 = 0$, $h_4 = 0$, $h_5 = 1.4$, $h_6 = 0$, $h_7 = 0$, $h_8 = 0.98$, $h_9 = 0$, $l_1 = 1.195$, $l_2 = 0.836$, $l_3 = 0.585$, $l_4 = 0.409$

following the same values. Conversely, for ②, the values of E_s are smaller, the simulation stops due to joint limits, and the three angles α_i increase separately until they reach an angle limited by the minimum length of each spring. At this point, the simulation stops because the optimization cannot converge.

To have a more homogeneous behavior, to make α_i the same for all segments, we had to change the spring rate. This means that we have to formulate a new E_s:

$$\begin{aligned} E_{s'} = & \frac{1}{2}\left(k_1(\rho_1 - l_{01})^2 + k_2(\rho_2 - l_{02})^2\right) \\ & + \frac{1}{2}\left(\frac{k_3}{\lambda}(\rho_3 - l_{03})^2 + \frac{k_4}{\lambda}(\rho_4 - l_{04})^2\right) \\ & + \frac{1}{2}\left(\frac{k_5}{\lambda^2}(\rho_5 - l_{05})^2 + \frac{k_6}{\lambda^2}(\rho_6 - l_{06})^2\right) \end{aligned} \tag{17}$$

Figure 9 depicts the impact of the spring properties. When the spring stiffness is increased by multiplication by $1/\lambda$ for ® and $1/\lambda^2$ for ©, the energy variation becomes the same as in ① as well as the change in angles $\alpha_{123'}$.

A non-optimal solution was also studied. The shape is similar to ② but with offsets between the pivot joints (A_0, B_0), (D_0, E_0), (F_0, H_0) and (I_0, J_0) (Fig. 10). We note this example, ④.

Taking into account the no-load length of the springs, the angular displacement obtained by ④ is comparable to ① and the

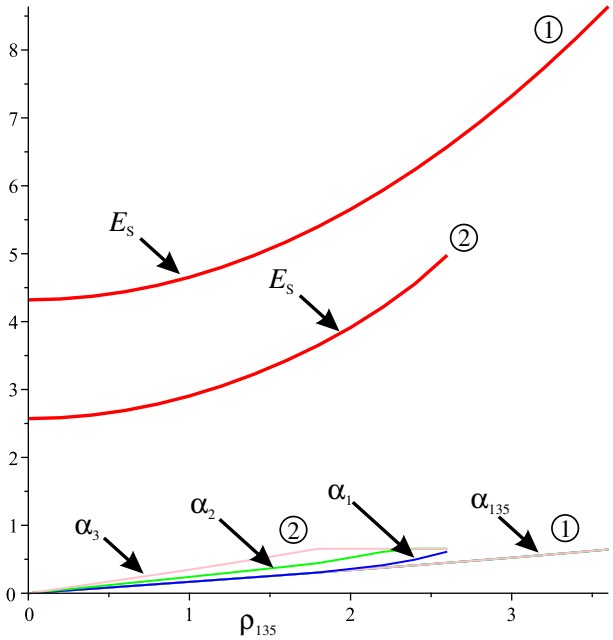

FIGURE 8. Variation of E_s as a function of ρ_{135} for the both designs with $k_i = 1$

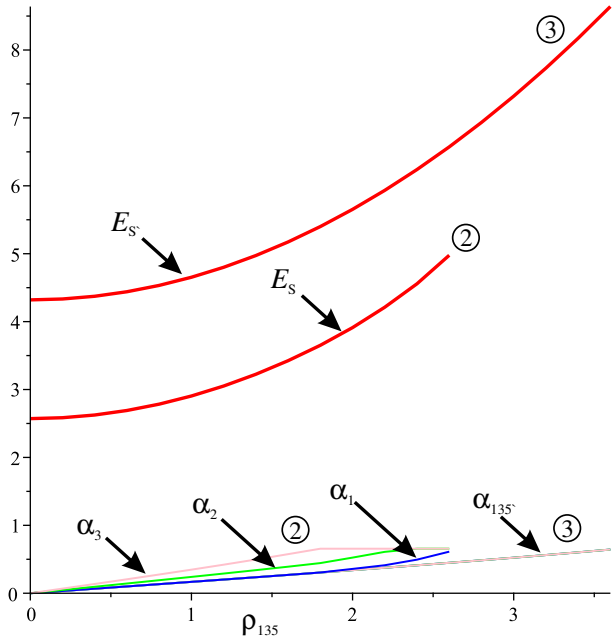

FIGURE 9. Variation of E_s and $E_{s'}$ as a function of α_i for the mechanism ② with identical springs and ③ with adjusted springs $k_i = 1$

simulation stops at about the same value.

CONCLUSIONS AND FUTURE WORK

In this paper, a mechanism consisting of a stack of three tensegrity mechanisms was studied. This mechanism was studied with an objective to serve as a stapler for laparoscopic surgeries for rectal cancer and other coloanal procedures, where conventional tools cannot be easily accessed. The mechanism consists of rigid bodies, pivots with paired movements, linear springs, and cables for actuation. Parallel singularities were analyzed as well as stability using the minimum energy principle. An optimization was made to obtain the largest angular deflection based on a ratio λ between the size of the base and the platform.

Optimal design parameters were found for which the angle α can vary between $-\pi/2$ and $\pi/2$. We found that when the size of the base and platform are identical, i.e. when $\lambda = 1$, the total energy in a module is minimal.

Using an optimization function, the deformation of the mechanism as a function of the length of a cable was observed for several design parameters. We observe that the no-load length of the springs has great importance in the mobility of the mechanism and that the effects of a size variation between the segments can be compensated by changing the stiffness properties of the springs.

Further researches are underway to evaluate the number of segments to be used for a stapler to achieve the required curvature during the laparoscopic surgical procedure and effectively

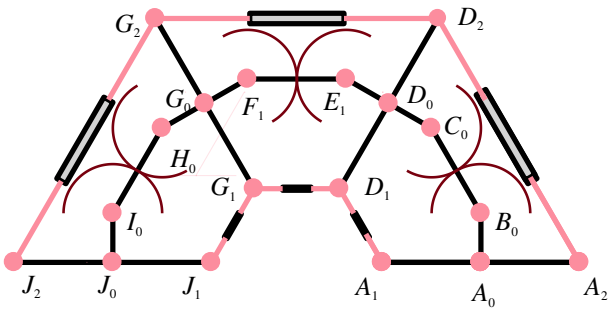

FIGURE 10. Example of a bending mechanism with $h_1 = \frac{1}{2}$, $h_2 = 1$, $h_3 = \frac{1}{2}$, $h_4 = \frac{1}{2}$, $h_5 = 1$, $h_6 = \frac{1}{2}$, $h_7 = \frac{1}{2}$, $h_8 = 1$, $h_9 = \frac{1}{2}$, $l_1 = 1$, $l_2 = 1$, $l_3 = 1$, $l_4 = 1$

separate the tissue with minimum trauma while keeping the mechanism as simple as possible. A stability study will also need to take into account the influence of the stiffness of the cutting knife and the mechanism by which it moves. A coupling between the vertebrae with a flexible element is also being studied to replace the coupled revolute joints. In this case, flexible mechanism modeling tools will be used in addition to studies on tensegrity mechanisms.

REFERENCES

[1] A. D. Gaidry, L. Tremblay, D. Nakayama, and R. C. Ignacio, "The History of Surgical Staplers: A Combination of Hun-

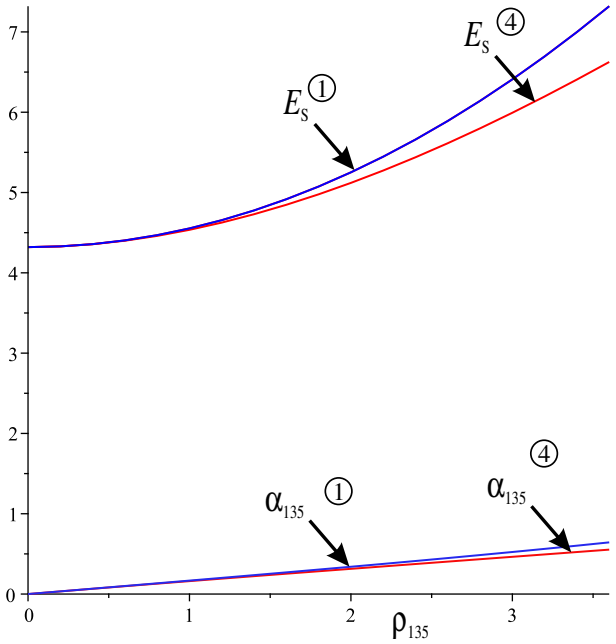

FIGURE 11. Variation of E_s as a function of ρ_{123} for mechanism ① and ④

garian, Russian, and American Innovation," *The American Surgeon*, vol. 85, pp. 563–566, jun 2019.

[2] A. Akopov, D. Y. Artioukh, and T. F. Molnar, "Surgical Staplers: The History of Conception and Adoption," *The Annals of Thoracic Surgery*, vol. 112, pp. 1716–1721, nov 2021.

[3] E. Chekan and R. Whelan, "Surgical stapling device-tissue interactions: what surgeons need to know to improve patient outcomes," *Medical Devices: Evidence and Research*, vol. 7, p. 305, sep 2014.

[4] S. Kostrzewski, E. Aranyi, and P. Scirica, "IN-SITU LOADED STAPLER," US Patent 9364217B2, 2016.

[5] R. D. Adams, Holliston, L. O. Main, Loveland, S. E. Swaffar, Bloomington, and Charles H. Pugsley, "ENDOSCOPC STAPLER," US Patent 6302311, 2001.

[6] K. M. Tobias, "Surgical Stapling Devices in Veterinary Medicine: A Review," *Veterinary Surgery*, vol. 36, pp. 341–349, jun 2007.

[7] P. Schemmer, H. Friess, C. Dervenis, J. Schmidt, J. Weitz, W. Uhl, and M. W. Büchler, "The Use of Endo-GIA Vascular Staplers in Liver Surgery and Their Potential Benefit:A Review," *Digestive Surgery*, vol. 24, no. 4, pp. 300–305, 2007.

[8] H. Bolanos, E. Norwalk;, C. R. Sherts, Southport;, A. T. Pelletier, and Wallingford, "ENDOSCOPIC STAPLER," US Patent 690269, 1997.

[9] K. L. Milliman, Bethel;, F. J. Viola, S. Hook;, J. Orban, Norwalk;, R. F. Lehn, and Stratford, "SURGICAL STAPLING APPARATUS," US Patent 586531, 1999.

[10] T. Ema, "The experience of using Endo GIA™ Radial Reload with Tri-Staple™ Technology for various lung surgery," *Journal of Thoracic Disease*, vol. 6, no. 10, pp. 1482–1484, 2014.

[11] D. E. Rivadeneira, J. C. Verdeja, and T. Sonoda, "Improved access and visibility during stapling of the ultra-low rectum: a comparative human cadaver study between two curved staplers," *Annals of Surgical Innovation and Research*, vol. 6, p. 11, dec 2012.

[12] L. de Calan, B. Gayet, P. Bourlier, and T. Perniceni, "Chirurgie du cancer du rectum par laparotomie et par laparoscopie," *EMC - Chirurgie*, vol. 1, pp. 231–274, jun 2004.

[13] G. Ruffo, A. Sartori, S. Crippa, S. Partelli, G. Barugola, A. Manzoni, M. Steinasserer, L. Minelli, and M. Falconi, "Laparoscopic rectal resection for severe endometriosis of the mid and low rectum: Technique and operative results," *Surgical Endoscopy*, vol. 26, no. 4, pp. 1035–1040, 2012.

[14] M. Furet, M. Lettl, and P. Wenger, "Kinematic Analysis of Planar Tensegrity 2-X Manipulators," in *International Symposium on Advances in Robot Kinematics*, vol. 8, pp. 153–160, Springer, 2018.

[15] P. Wenger and D. Chablat, "Kinetostatic analysis and solution classification of a class of planar tensegrity mechanisms," *Robotica*, vol. 37, pp. 1214–1224, jul 2019.

[16] F. Rouillier, "Solving Zero-Dimensional Systems Through the Rational Univariate Representation," *Applicable Algebra in Engineering, Communication and Computing*, vol. 9, pp. 433–461, may 1999.

[17] S. Behzadipour and A. Khajepour, "Stiffness of Cable-based Parallel Manipulators With Application to Stability Analysis," *Journal of Mechanical Design*, vol. 128, pp. 303–310, jan 2006.

[18] T. Chadefaux, "The Triggers of War: Disentangling the Spark from the Powder Keg," *SSRN Electronic Journal*, pp. 1–42, 2014.

[19] W. Zhao, A. Pashkevich, A. Klimchik, and D. Chablat, "Elastostatic Modeling of Multi-Link Flexible Manipulator Based on Two-Dimensional Dual-Triangle Tensegrity Mechanism," *Journal of Mechanisms and Robotics*, vol. 14, no. 2, pp. 1–31, 2022.

[20] J. Yang, E. P. Pitarch, J. Potratz, S. Beck, and K. Abdel-Malek, "Synthesis and analysis of a flexible elephant trunk robot," *Advanced Robotics*, vol. 20, no. 6, pp. 631–659, 2006.